Korean J. Chem. Eng., 32(8), 1625-1633 (2015)
DOI: 10.1007/s11814-014-0375-x

pISSN: 0256-1115
eISSN: 1975-7220

A novel sintered metal fiber microfiltration of bio-ethanol fermentation broth

Qian Kang*,, Jan Baeyens**,†, Tianwei Tan**, and Raf Dewil***

*Department Chemical Engineering, Process and Environmental Technology Lab., KU Leuven, Sint-Katelijne-Waver, Belgium
**School of Life Science and Biotechnology, Beijing University of Chemical Technology, Beijing, China
(*Received 24 June 2014 • accepted 17 December 2014*)

Abstract−In bio-ethanol fermentation, the broth consists of mainly water and ethanol, together with particulate residues of unreacted feedstock and additives (mostly yeast). Prior to further processing (distillation), and to avoid fouling of heat exchangers and distillation columns, the solids residues of the broth need to be removed to as low a concentration as possible. The current mechanical separation (belt filter or centrifuge) can only remove +10 μm particles representing about 90% of the total solids content. The remaining 10% is usually recovered in the bottom stream of the first distillation column, and forms the stillage that is further treated. To avoid fouling and even eliminate the first distillation column where the ethanol fraction is only increased from 12% (feed) to 16% (top), a better particulate removal is required. Novel sintered metal fiber (SFM) fleeces are highly efficient for microfiltration, and the removal of suspended solids largely exceeds 99%. The paper (i) positions microfiltration in the overall bio ethanol process; (ii) describes the novel sintered metal fiber microfiltration application; (iii) experimentally determines the major operating characteristics of SFM and (iv) predicts the up-scaled operation by using a simplified filtration model. At an ambient feed temperature, the flux of permeate exceeds 5 m^3/m^2h for a TMP of 1.5 bar and a yeast concentration of 15 g/*l*, as commonly encountered in the fermenter broth.

Keywords: Bioethanol, Microfiltration, Sintered Metal Fleece, Models

INTRODUCTION

1. Bio-ethanol Process

Bioethanol, as a clean and renewable fuel, is gaining increasing attention. It can be produced from different types of renewable feedstock, such as corn, wheat, sugar cane, cassava (first generation), cellulose biomass (second generation) and algal biomass (third generation). Different key parts of the bio-ethanol process for the three generations of feedstock are identical and presented in Fig. 1, the difference being a required pretreatment of the second and third generation feedstock. Fermentation, distillation, dehydration and residue/wastewater treatments are common to all processing schemes. Steam is required in pre-treatment, saccharification, distillation, dehydration and residue drying.

To produce ethanol from starchy materials such as cereal grains or cassava, the starch must first be hydrolyzed into sugars (glucose) by either a chemical treatment (using dilute sulfuric acid); or biologically (by fungally produced amylase); or by the combination of both [1]. Some processes, e.g., Lurgi [2], separate the enzymatic saccharification and fermentation, while other processes, such as Cofco [3,4], combine gluco-amylase and *Saccharomyces cerevisiae* within a single fermenter. The Cofco batch fermentation process usually takes up to 65 h. The initial mash-suspension to which amylase is added contains cassava and water in a ratio of 1-2.5, for an initial cassava content of 28,6 wt% [3,4]. The cassava starch-content of approximately 70% and the conversion efficiency of 90% provide an ethanol yield of 63% of the cassava feed. Specific problems of ethanol inhibition (at ~120 g/*l*) are counteracted in some novel processes by using, e.g., *Zymomonas mobilis* that succeeds to survive higher ethanol concentrations in the fermenter, has a high tolerance for acids and sugars, enhances the fermentation rate [5], and was the basis of very high gravity fermentation (VHG).

2. Mass Balance of the Bio-ethanol Production, and Potential of Membrane Separation

Referring to the flowsheet of Fig. 1, the Cofco [3,4] plant operates six fermenters in parallel, each with a volume of 3,025 m^3 and with individual cassava feed of 865 ton. The mass balance of a single fermenter is given in Fig. 2. The amount of starch converted is 549 tons. Fermenter solids (mostly cassava residue, yeasts) are removed from the broth by traditional centrifuge or belt filter at 90% mechanical separation efficiency. The remaining 10% of the solids (mostly yeasts) are carried forward to the distillation and are responsible for heat exchanger fouling and the production of a very dilute stillage in the first distillation column. To keep the population of yeast (*Saccharomyces*) or bacteria (*Zymomonas*) at a required high level, part of the separated solids are recycled to the fermenter.

For the total Cofco process, the production capacity is ~200,000 tpa of anhydrous ethanol. Since this capacity is the average of the current commercial range (50,000 to 400,000 tpa), we have selected 200,000 tpa as typical capacity. After the mechanical separation, the solid residue of 32 ton in a total liquid flow of 2,365 ton corresponds to a concentration of ~14 g/L.

A recent review [6] summarizes the state-of-the art of different membrane applications in the bio-ethanol process, being of different nature and mostly focused upon the targets listed in Table 1. Referring to the process diagram of Fig. 1, the major applications

†To whom correspondence should be addressed.
E-mail: baeyens.j@gmail.com

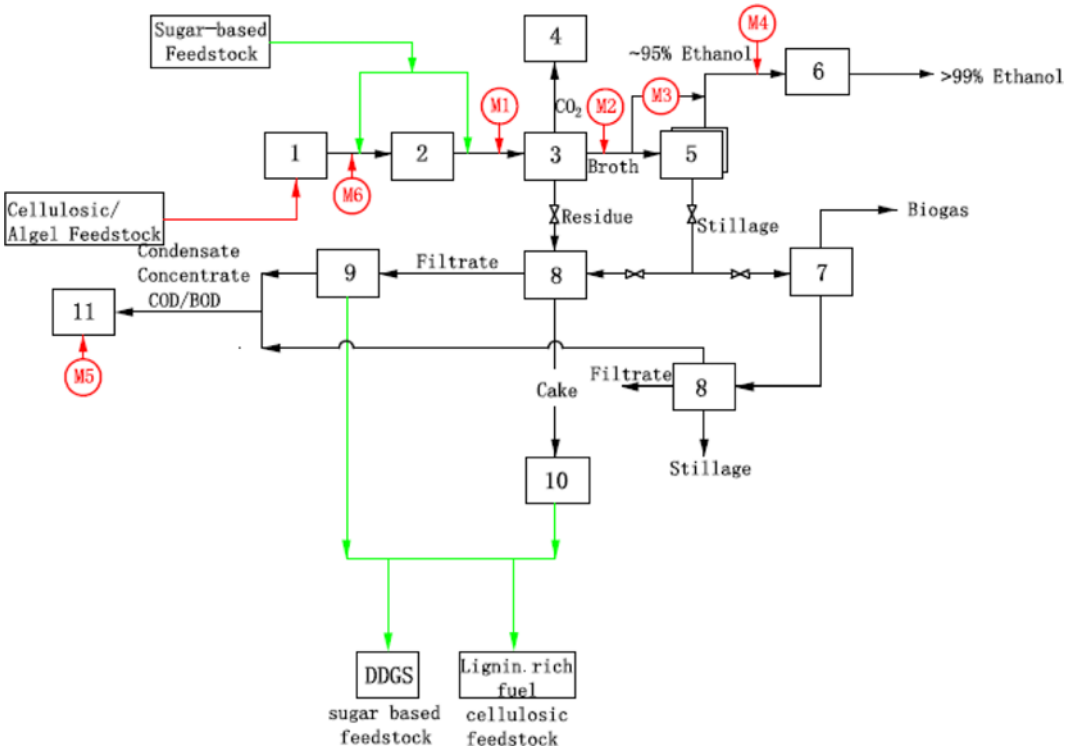

Fig. 1. Schematics of the processes for bio-ethanol production as currently applied (DDGS: Distillers Dried Grains with Solubles). (a) As currently applied; (b) With potential membrane application.

(a): 1. Pre-treatment
2. Hydrolysis and/or Saccharification
3. Fermentation
4. CO_2 scrubbing
5. Distillation
6. Ethanol dehydration
7. Anaerobic digestion
8. Mechanical dewatering
9. Evaporation
10. Dryer
11. Anaerobic wastewater treatment

(b): M1, M2. Microfiltration
M3, M4. Pervaporation
M5. Combined membrane processes
M6. Ultrafiltration, nanofiltration, reverse osmosis

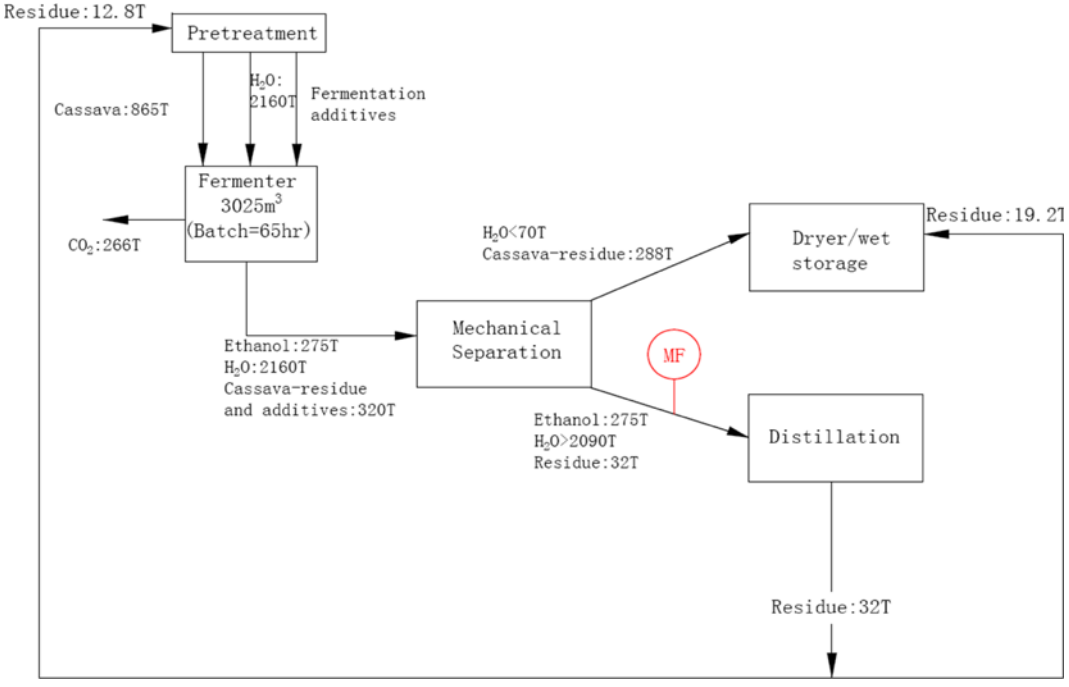

Fig. 2. Mass balance of the process of cassava-based bioethanol production (MF: added microfiltration).

Table 1. Possible membrane applications in bio-ethanol production

Membrane technique	Application
Microfiltration [10-12]	- In microalgae harvesting - To complete the traditional broth mechanical separation - To protect subsequent pervaporation, distillation columns and heat exchangers from fouling - In the treatment of effluent treatment streams
Pervaporation [13-18]	- To reduce the distillation energy consumption, often as hybrid operation - To dewater ethanol after the 95 m% azeotrope
Reverse osmosis/nanofiltration [19-24]	- In removing inhibitors after saccharification - For sugar concentration
Ultrafiltration [25-27]	- To recycle micro-organisms and other value-added chemicals such as cellulase in the enzymatic hydrolysate

of microfiltration are situated at different levels, i.e. (i) in the harvesting and pre-treatment of algal biomass, hence in item [1]; (ii) to filtrate the broth before the distillation (and pervaporation, in a hybrid system), hence after item [3]; and (iii) to perform a final filtration step of the wastewater treatment, hence integrated in item [7]. The benefits of introducing membrane techniques are now recognized, although extensive research is still needed to scientifically and economically justify their application. The present paper will only consider microfiltration, with pervaporation and dewatering membranes reported upon elsewhere [8,9].

3. Microfiltration and Sintered Metal Microfilters

Early membranes were isotropic structures with uniform properties across the entire membrane. They have been thoroughly investigated and widely applied. Polymer, powdered metal or ceramic membranes belong to this early microfiltration development. Their thickness and associated TMP are generally considerable and their normalized water permeability (NWP), the clean water permeate flux at a TMP of 1 bar and at 25 °C is rather low (<500 L/m^{2}hbar). Novel membranes have an anisotropic structure consisting of a thin, dense layer, typically 0.1-0.2 mm thick, supported by a much more open and permeable layer, also of a similar thickness. This support layer provides sufficient mechanical strength to allow the membrane to be manufactured into common geometries (e.g., plates or candles) and to be easily handled. By making the selective layer thin, high permeate flow rates are obtained, generally with a NWP in excess of 10,000 L/m^{2}hbar.

Sintered metal fiber microfilters belong to the anisotropic class. Metal fibers used in these filter media, range in diameter from 1 μm to 10 μm and are available in different alloys (AISI 316L, Hastalloy, Inconel, Fecralloy, Ni or Ti) to meet specific applications. The enhanced surface filtration medium (SFM) [28], uses short fibers with an L/D ratio of about 100, A final product, mechanically supported by several meshes, is obtained after sintering in a reducing atmosphere. The thin and fine upper filtration layer prevents the particles from penetrating the medium with subsequent clogging and corrosion (e.g., pitting damage, stress corrosion cracking) [28] as a result. SFM filters use fine fibers, have a low thickness of the fleece, and a fair to excellent permeability: fiber diameters of 1.25 to 6.35 μm are commonly used, for a fleece thickness of about 0.5 mm, with a porosity in excess of 60% and a weight of ~400 g/m^2.

The membrane used in the present investigations was an anisotropic membrane with successive layers of 1.25 μm (217 μm thick), 4 μm (144 μm thick) and 6 μm (289 μm thick). The finest mesh forms the selective layer. The NWP was ~21,000 L/m^{2}hbar.

4. Objectives of the Paper

The research here is limited to application of SFM microfiltration within the process of fermentative bioethanol production. The objectives of the paper are threefold: (i) position the potential of using microfiltration in the overall biochemical process of bio-ethanol, using the Cofco plant [3,4] as a case-study; (ii) describe the novel sintered metal fiber microfiltration application, and (iii) through initial experiments and modelling, determine the major operating characteristics of sintered metal microfiltration.

MATERIALS AND METHODS

1. Particulate Characteristics of the Fermentation Broth

A laboratory-simulated corn-based fermenter broth was subjected to a particle size measurement using a Cilas 920. The broth solid residue consists of non-converted feedstock and mainly yeast, with <10 μm solids being mostly yeasts and enzymes.

2. Sintered Metal Microfilters

Sintered metal fiber units in AISI 316L were used. The SFM 1.3 has a fiber diameter of 1.25 μm as the selective layer, with 4 and 6 μm fiber as supporting mesh (see 1.3).

3. Experimental Layout and Procedure of Cross-flow Filtration Experiments

The experimental layout is illustrated in Fig. 3. Temperatures were held constant at 20 °C. Concentrate and permeate are recycled to the feed tank to maintain a nearly constant feed concentration during the experiment.

The microfiltration module contains three parallel sintered metal fiber elements, each of effective filtration surface of 0.0175 m^2, and illustrated in Fig. 4. The back pulse cleaning is operated periodically (in function of the tolerated and pre-set maximum feed pressure). In the experimental unit, the back pulse cake is recycled to the feed tank to maintain a constant feed concentration. The back pulse occurred at a given time interval (5 to 30 seconds) by using an air-pressurized (4 to 6 bar) permeate flow during 100 to 200 msec.

To investigate the use of this novel microfiltration in the production process of bio-ethanol, experiments were carried out with a yeast (d<12 μm) suspension as representative sample of the fer-

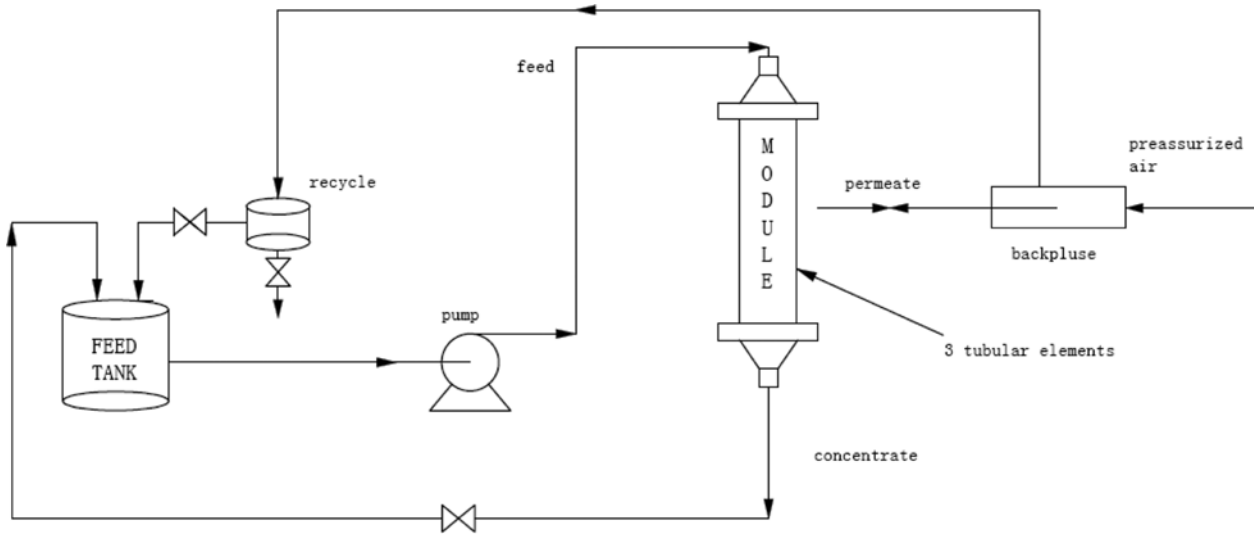

Fig. 3. Experimental set-up with 3-tubular Microfiltration elements.

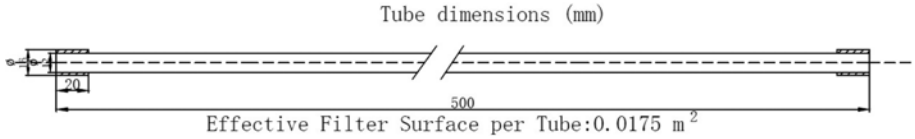

Fig. 4. Geometry of a single sintered metal fiber filter element.

mented broth after pre-mechanical separation, tested at transmembrane pressures (TMP) between 0.2 and 1.5 bar, at concentrations from 3 to 100 g/*l* and at tangential velocities up to 8 m/s.

RESULTS

1. Particle Characteristics of the Fermenter Broth

Results, illustrated in Fig. 5, demonstrate that traditional particle separation techniques, with a cut-size of 10 μm, can indeed only separate about 80% of the suspended particles.

The residual 10 to 20% is usually separated in the bottom stream of the first distillation column and forms the stillage. If microfiltration were to be used, it would need to also separate the ≤10 μm particles.

2. Particulate Removal by Microfiltration

Irrespective of the operating conditions, the membranes tested were nearly total barriers for the suspended solids, with a >99% retention (<1% of the feed particulates were measured in the filtrate, as determined by filtration on a 45 nm Sartorius polyestersulfon filter after vacuum drying and weighing).

3. SFM-membrane Microfiltration Results

Experimental results for different operating conditions are illus-

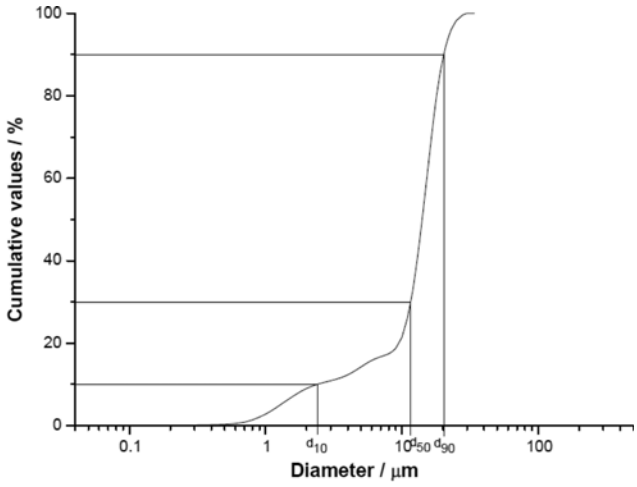

Fig. 5. Size analysis of broth particulates.

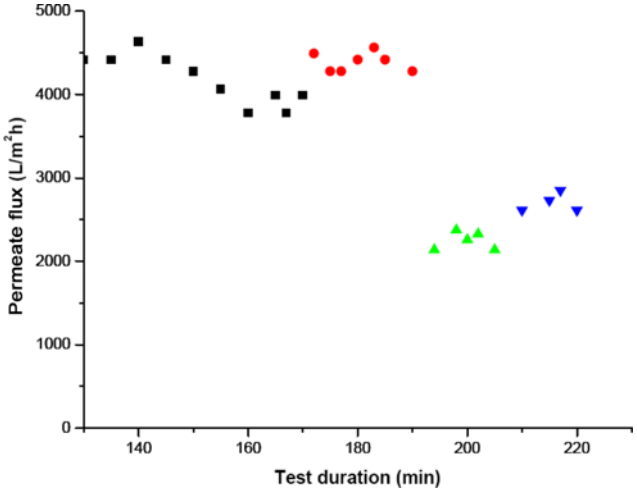

Fig. 6. Permeate flux at different interval of back pulse every ● 5 s, ■ 10 s, ▼ 20 s, ▲ 30 s.

trated below. The effect of the back pulse frequency is illustrated in Fig. 6, at a yeast concentration of 30 g/L.

A higher back pulse frequency is clearly more effective in removing the deposited cake, although an interval of 5 to 10 seconds appears to have the same effect. For a lower yeast concentration, the back pulse frequency could be increased to 1/30 sec, whereas at 100 g/L a back pulse every 10 sec proved to be adequate.

The effect of the TMP, as controlled by the feed pressure, is shown in Fig. 7. A higher TMP results in a higher obtainable permeate flux at a given back pulse frequency. The decreasing permeate flux with test duration at higher TMP indicates some degree of membrane clogging, with particles insufficiently removed by back pulsing.

The effect of the tangential velocity is less pronounced as illustrated in Fig. 8. Operation at higher tangential velocity value moreover increases the required volumetric flow rate of the feeding pump, with a resulting higher power consumption.

The effect of the yeast concentration in the required back pulse frequency is illustrated in Fig. 9. At higher yeast concentration, a higher back pulse frequency is required to maintain a high permeate flux.

The effects of TMP and back pulse frequency are illustrated in Fig. 10. Whereas back pulse frequency has a limited effect at low values of TMP, it is important to increase the frequency at higher TMP-values, again due to irreversible membrane clogging by the particles.

The effect of the tangential velocity is illustrated in Fig. 11(a)/(b), with higher tangential velocities being favorable towards a higher permeate flux. These higher values, leading to a higher shear on the deposited cake, will however remove part of the cake. This will be demonstrated in the model approach (Section 4) of the paper.

Finally, overall results at a back pulse every 10 sec, and a tangential velocity of 5.1 m/s, are illustrated in Fig. 12.

No significant variation of TMP could be seen during the dura-

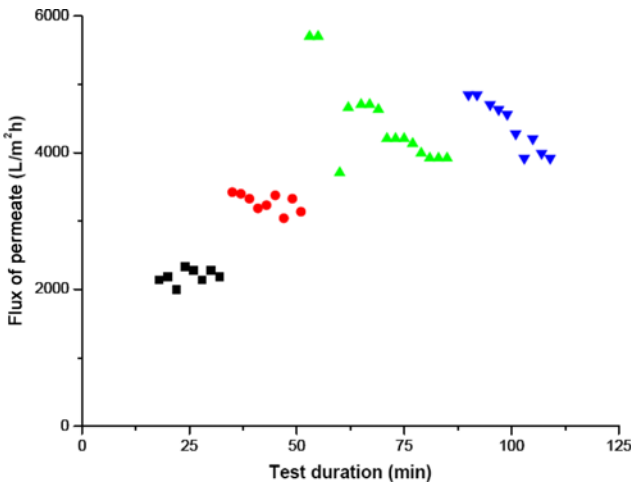

Fig. 7. Permeate flux at different TMP (■ 0.3 bar, ● 0.5 bar, ▲ 1 bar, ▼ 1.5 bar) (tangential velocity: 5.2 m/s; concentration of yeast: 30 g/L; back flushing every 10 sec).

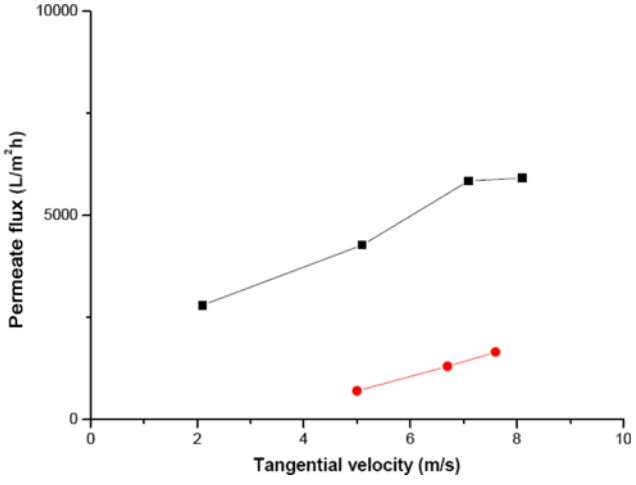

Fig. 8. Permeate flux versus tangential velocity at ■ 30 g/L and ● 100 g/L yeast.

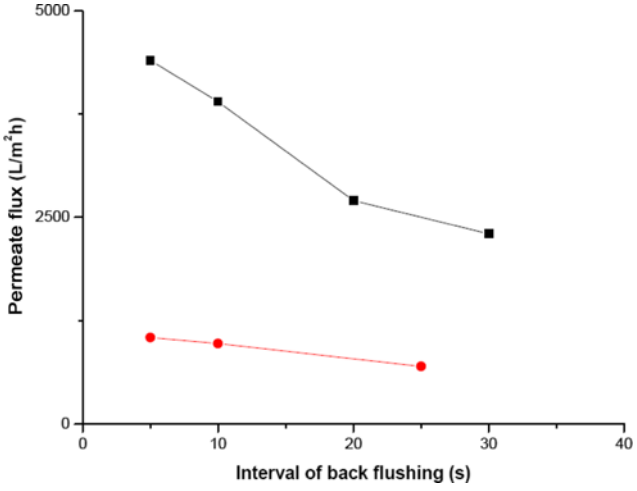

Fig. 9. Permeate flux versus interval of back flushing at ■ 30 g/L and ● 100 g/L yeast.

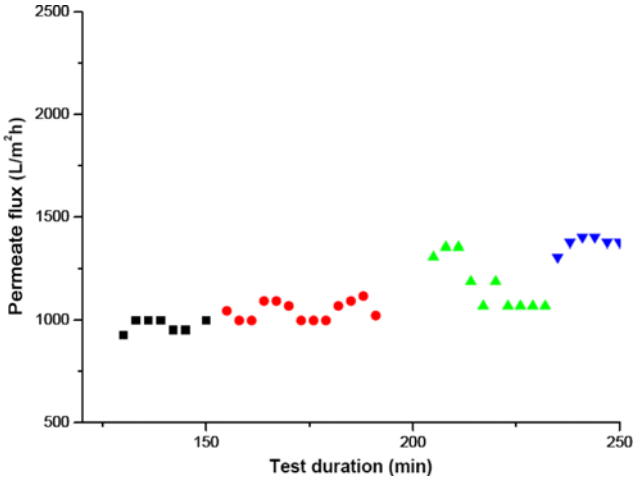

Fig. 10. Permeate flux at different TMP and interval of back flushing (■ 0.3 bar and 10 s; ● 0.5 bar and 5 s; ▲ 1 bar and 10 s; ▼ 1.5 bar and 5 s) (tangential velocity: 5.2 m/s; concentration of yeast: 100 g/L).

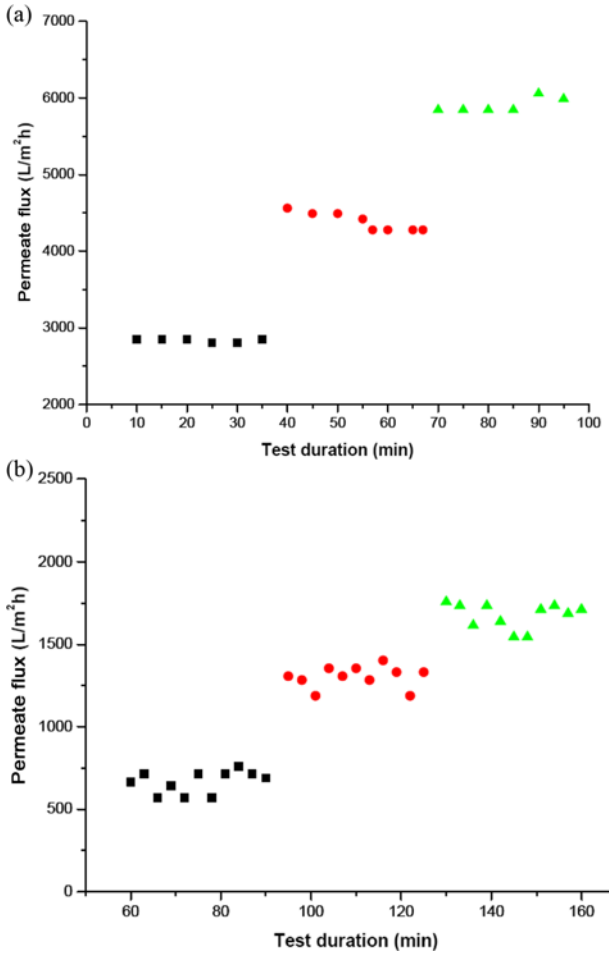

Fig. 11. (a) Permeate flux at different tangential velocities (■2.1 m/s; ● 5.1 m/s; ▲ 7.1 m/s) (TMP=0.5 bar; concentration of yeast: 30 g/L; back flushing every 10 sec). (b) Permeate flux at different tangential velocities (■ 5 m/s; ● 6.7 m/s; ▲ 7.6 m/s) (TMP=0.5 bar; concentration of yeast: 100 g/L; back flushing every 10 sec).

tion of the test, indicating that the back-pulse cleaning was effective and that no yeast particles penetrated and clogged the membrane fleece, to slowly build up pressure.

MODEL APPROACH

1. Empirical Models

Different models have been reviewed in literature, as presented

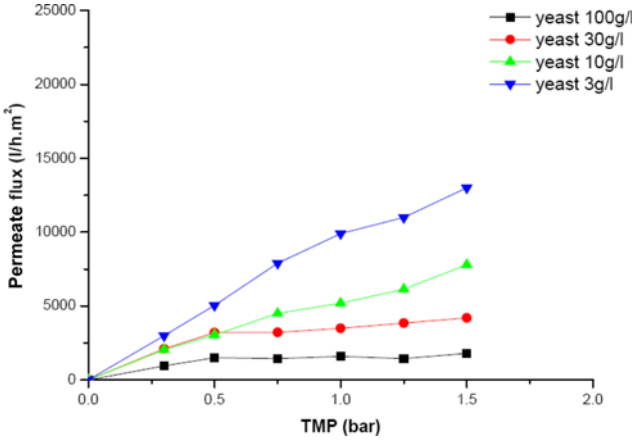

Fig. 12. Experimental results for yeast suspensions of a SFM 1.3-membrane.

Table 1. Empirical models [29]

Model	Comparison
Complete blocking model	$Q_0 - Q = K_p \cdot V$
Intermediate blocking model	$\frac{1}{Q} - \frac{1}{Q_0} = K_i \cdot t$
Standard blocking model	$\sqrt{Q_0} - \sqrt{Q} = K_s \cdot \sqrt{Q_0} \cdot V$
Cake filtration model	$\frac{1}{Q} - \frac{1}{Q_0} = K_c \cdot V$

in Table 2. Empirical results enable to determine the fitting parameters for a given permeate volume (V) obtained at time (t) for a given permeate flow rate Q_0 (initial) and Q (at time t). K_p, K_i, K_s and K_c are filtration constants of each respective model.

This has been applied for a yeast concentration of 5 and 50 g/L, respectively. Although all models can fit the experimental data fairly well at low values of time, deviations increase with increasing time, as shown in Figs. 13 and 14.

The use of the empirical models moreover requires the determination of the filtration constants, specific for each yeast concentration. A general application for design and scale-up is hence impossible.

2. Phenomenological Model Approach

To expand the use of the experimental results to different suspensions and in scaling-up, a model was developed, based upon the stagnant film theory (Fig. 15). The model predicts the steady-state permeate flux of cross-flow microfiltration. The permeate

Table 2. Application of models for different yeast concentration

Model	Yeast 5 g/L	Yeast 50 g/L
Complete blocking model	$0.013 - Q = 0.0009 \cdot V$	$0.01 - Q = 0.002 \cdot V$
Intermediate blocking model	$\frac{1}{Q} - \frac{1}{0.013} = 0.0814 \cdot t$	$\frac{1}{Q} - \frac{1}{0.01} = 0.2571 \cdot t$
Standard blocking model	$\sqrt{0.013} - \sqrt{Q} = 0.0045 \cdot \sqrt{0.013} \cdot V$	$\sqrt{0.01} - \sqrt{Q} = 0.0118 \cdot \sqrt{0.01} \cdot V$
Cake filtration model	$\frac{1}{Q} - \frac{1}{0.013} = 5.0961 \cdot V$	$\frac{1}{Q} - \frac{1}{0.01} = 30.942 \cdot V$

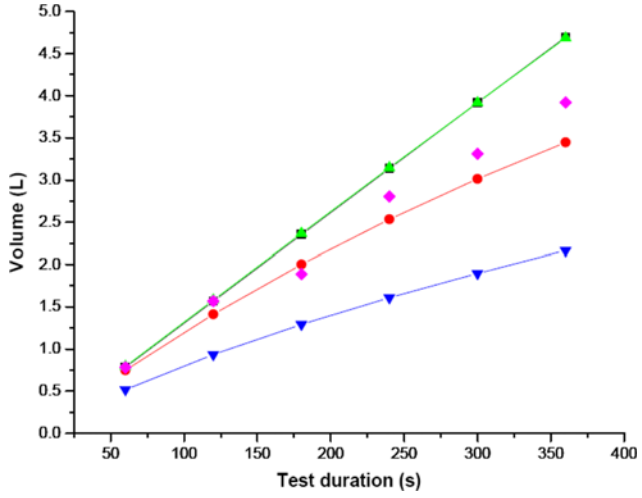

Fig. 13. The comparison of model and experimental data at yeast 5 g/L (■ complete blocking model; ● intermediate blocking model; ▲ standard blocking model; ▼ cake filtration model; ◆ experimental data).

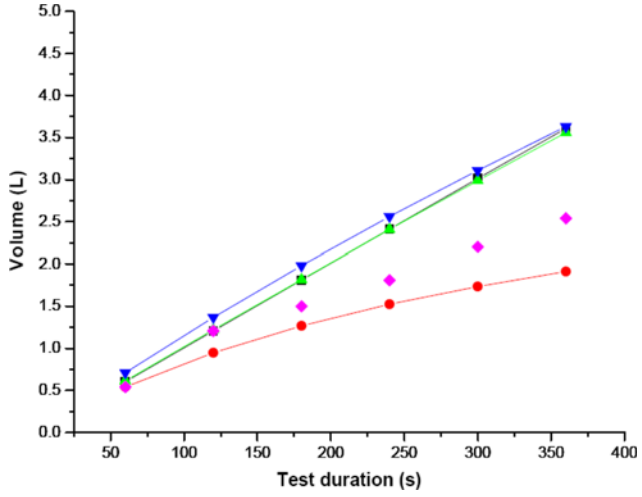

Fig. 14. The comparison of model and experimental data at yeast 50 g/L (■ complete blocking model; ● intermediate blocking model; ▲ standard blocking model; ▼ cake filtration model; ◆ experimental data).

passes through the filter and the accumulated particles on the surface of the filter form a cake-layer. Because of the shearing of the filter by the tangential liquid flow, this cake-layer is partly removed and returned back to the bulk of the feed. The model consists of three basic equations:

- mass flux-transport towards the filter surface,

$$m = J \cdot c_b \tag{1}$$

- Darcy's law

$$J = \frac{\Delta P}{\eta (R_c + R_m)} \tag{2}$$

- the mass flux-transport towards the bulk of the feed by the tangential velocity gradient [30]

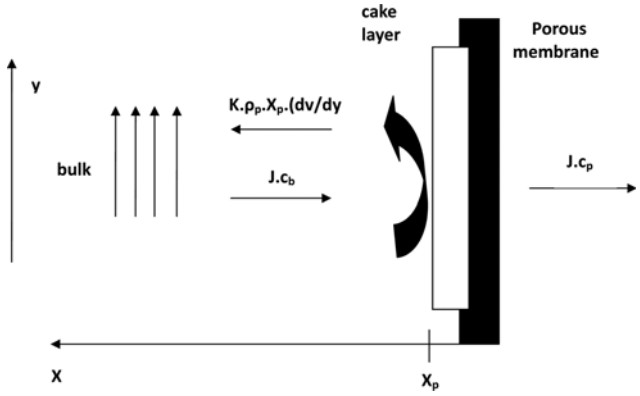

Fig. 15. Model based upon the stagnant film theory.

$$\text{For laminar flow, } m = K \cdot \rho_p \cdot x_p \cdot \frac{dv}{dy} \text{ with } \frac{dv}{dy} = \frac{\tau}{\eta} \text{ [30]} \tag{3}$$

$$\tau = 8 \cdot \frac{\eta}{d} \cdot v \tag{4}$$

This results in the following equation for laminar flow and $R_c >> R_m$,

$$J = \sqrt{\frac{K \cdot \Delta P \cdot \rho_p \cdot v}{\eta \cdot r_c \cdot d \cdot c_b}} \tag{5}$$

with symbols defined before.

$$\text{For turbulent flow, Schulz et al. [30] define } \tau = \rho_f \cdot v^2, \tag{6}$$

resulting in

$$J = \sqrt{\frac{K \cdot \Delta P \cdot \rho_p \cdot \rho_f}{r_c \cdot c_b}} \cdot \frac{\upsilon}{\eta} \tag{7}$$

From Eq. (5) one can determine the constant K according to

$$K = \frac{J^2 \cdot \eta \cdot r_c \cdot d \cdot c_b}{\Delta P \cdot v \cdot \rho_p} \text{ (in laminar flow)} \tag{8}$$

$$\text{or } K = J^2 r_c c_b \left(\frac{\eta}{\nu}\right)^2 \cdot \frac{1}{\Delta P \cdot \rho_\rho \cdot \rho_f} \text{ (in turbulent flow)} \tag{9}$$

with r_c determined by the Kozeny-Carman [31] equation:

$$r_c = 180 \frac{(1-\varepsilon)^2}{\varepsilon^3 \cdot (\phi_s \cdot d_p)^2} \tag{10}$$

The determination of the constant from a single experimental point permits the prediction of the flow rates for different velocities and applied pressures.

The flow regime is determined by the Reynolds-number defined in the bulk stream, i.e., in the concentric channel between the membrane candle and the container.

$$Re = \frac{\rho_f \cdot \upsilon \cdot d'}{\eta'} \tag{11}$$

where ρ_f is the fluid density (kg/m^3), approximately equal to the density of water in view of the low yeast concentration; υ is the tangential velocity (m/s); d′ is the characteristic size of the free section of fluid flow, about 0.003 m; η' is the viscosity of the liquid (kg/ms).

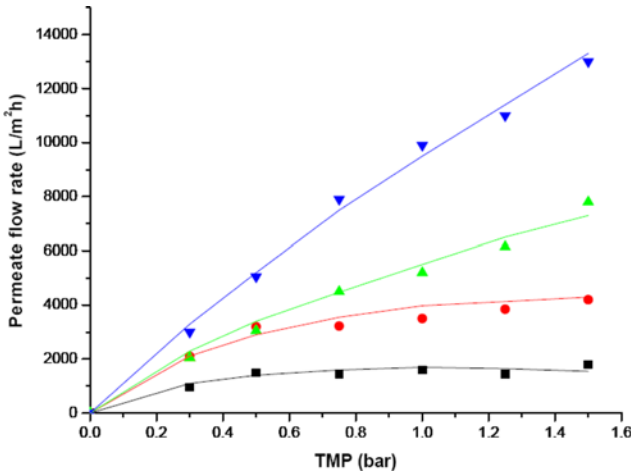

Fig. 16. Comparison of model predictions (— — — —) and experimental results (■ ● ▲ ▼) yeast 100 g/l: — ■; yeast 30 g/l: — ●; yeast 10 g/l: — ▲; yeast 3 g/l: — ▼.

With the common operating tangential velocities of 2 to 8 m/s, and with a viscosity of the yeast suspension of 5 cP ($5*10^{-3}$ kg/ms), the Reynolds number varies between 1200 and 4800, and is hence clearly of laminar nature for smooth permeable pipes [30].

The Kozeny-Carman Eq. (10) can be applied to calculate the cake resistance, with ε=0.389, the densest packing of spherical particles under pressure; Φ_s=particle sphericity, 0.8-0.9; d_p=average yeast particle size, assumed at 5 μm. With these parameters, $r_c=7.13*10^{13}$ m^{-2}.

Since the flow regime is of laminar nature, Eq. (5) can be used. A single experimental result is then needed to determine the specific constant K.

Using a yeast suspension of 30 g/L, at a tangential velocity of 7.1 m/s, the flux through a single channel at TMP=0.5 bar is $5.4*10^{-4}$ m^3/m^2s. The viscosity of the yeast suspension, at dilute concentrations, can be estimated at $5*10^{-3}$ kg/ms [4].

Using these data in Eq. (5), yields a K-value of $1.14*10^{-5}$, used throughout the predictions for other experimental conditions. These predictions are then compared with the experimental results (Fig. 16). The good comparison between the model predictions and the experimental results stresses the validity of the approach. Similar fitting results were obtained for different tangential velocities.

For the flow rate of 2,365 tons during a fermentation cycle of 65 hrs (see Fig. 2), the hourly flow rate to be dealt with by the microfiltration unit is ~37 m^3/hr. Using six parallel fermenters, the flow rate will be ~150 m^3/hr. Operating the membrane at a TMP of 1 bar, for a yeast concentration of 14 g/L, will permit a membrane permeation flux in excess of 5 m^3/m^2h, thus necessitating a microfiltration unit of at a maximum 30 m^2 only. Since fine yeast and debris particles will be removed, the risk of heat exchanger and distillation column fouling is overcome, and the first distillation column of the Cofco layout is no longer required. Investments in microfiltration unit will certainly be balanced by omitting the first distillation column.

CONCLUSIONS

The novel sintered metal membranes are highly efficient for microfiltration, and the removal of suspended solids is excellent. The flux reduction is essentially due to a particle deposition that can be significantly eliminated operating at higher driving pressures and cross-flow velocity. The optimization of the microfiltration process depends strongly upon the applied pressure, tangential velocity and backpulse-time. The cross-flow surface microfiltration can be described by using stagnant film theory. Model predictions and initial experimental results are in fair agreement.

ACKNOWLEDGEMENTS

This work was supported by the National Basic Research Program of China (973 program) (2013CB733600, 2012CB725200), the National Nature Science Foundation of China (21436002, 21390202), the National High-Tech R&D Program of China (863 Program) (2012AA021404, 2014AA021903, 2014AA021904), and Key Projects in the National Science & Technology Pillar Program during the 12th Five-year Plan Period (2011BAD22B04).

LIST OF SYMBOLS

m, J : mass flux (kg/m^2s) and permeate flux (m^3/m^2s), respectively
c_b : concentration in the bulk [kg/m^3]
ΔP : TMP, transmembrane pressure [Pa]
η : dynamic viscosity [Pa s]
R_m, R_c : membrane and cake resistance [*l*/m]
K : filtration constant [-]
r_c : specific cake resistance [*l*/m^2]
ρ_p : particle density [kg/m^3]
x_p : cake thickness [m]
dv/dy : tangential velocity gradient [1/s]
v : tangential velocity [m/s]
y : axial distance [m]
τ : shear stress [Pa]
d, d_p : tube and particle diameter, respectively [m]
ε : cake porosity [-]
Q_0 : initial permeate flow rate [L/s]
Q : permeate flow rate at time t [L/s]
t : time [s]
K_p, K_i, K_s, K_c : empirical constants of model approaches (Section 4.1) (L/s, 1/L, 1/L, s/L^2, respectively)
Re : Reynolds-number [-]
ρ_f : fluid density [kg/m^3]
d′ : characteristic size of the free section of fluid flow [m]
η' : viscosity of the liquid [kg/ms]
ϕ_s : particle sphericity [-]

REFERENCES

1. A. S. Amarasekara, Handbook of Cellulosic Ethanol, Wiley, New Jersey and Scrivener Publishing LLC, Massachusetts (2014).
2. Lurgi, Retrieved from http://gep-france.com/biocarb/Bioethanol-Lurgi.pdf (11/05/2014).
3. H. L. Zhang, J. Baeyens and T. W. Tan, *Energy*, **48**, 380 (2012).
4. H. L. Zhang, J. Baeyens and T. W. Tan, *Chem. Eng. Res. Des.*, **90**, 2122 (2012).

5. G. W. Choi, H. W. Kang, Y. R. Kim and B. W. Chung, *Biotechnol. Bioproc. Eng.*, **13**, 765 (2008).
6. P. Wei, L. H. Cheng, L. Zhang, X. H. Xu, H. L. Chen and C. J. Cao, *Renew. Sust. Energy Rev.*, **30**, 388 (2014).
7. J. B. Castaing, A. Massé, V. Séchet, N. E. Sabiri, M. Pontié, J. Haure and P. Jaouen, *Desalination*, **276**, 386 (2011).
8. Q. Kang, J. Huybrechts, B. Van der Bruggen, J. Baeyens, T. W. Tan and R. Dewil, *Sep. Purif. Technol.*, **136**, 144 (2014).
9. J. Baeyens, Q. Kang, L. Apples, R. Dewil, Y. Q. Lv and T. W. Tan, *Prog. Energ. Combust. Sci.* (2014), DOI:10.1016/j.pecs.2014.10.003.
10. F. Lipnizki, *Desalination*, **250**, 1067 (2010).
11. L. Christenson and R. Sims, *Biotechnol. Adv.*, **29**, 686 (2011).
12. L. Brennan and P. Owende, *Renew. Sustain. Energy Rev.*, **14**, 557 (2010).
13. M. Nomura, T. Bin and S. Nakao, *Sep. Purif. Technol.*, **27**, 59 (2002).
14. M. I. Kaseno and T. Kokugan, *J. Ferment. Bioeng.*, **86**, 488 (1998).
15. T. Ikegami, D. Kitamoto, H. Negishi, K. Haraya, H. Matsuda, Y. Nitanai, N. Koura, T. Sano and H. Yanagishita, *J. Chem. Technol. Biotechnol.*, **78**, 1006 (2003).
16. J. B. Haelssing, A. Y. Tremblay and J. Thibault, *Chem. Eng. Sci.*, **68**, 492 (2012).
17. L. Aouinti and M. Belbachir, *Appl. Clay. Sci.*, **39**, 78 (2008).
18. P. Peng, B. Shi and Y. Lan, *Sep. Sci. Technol.*, **46**, 234 (2010).
19. I. S. Han and M. Cheryan, *J. Membr. Sci.*, **107**, 107 (1995).
20. S. Liu, T. E. Amidon and D. C. Wood, *J. Biobased. Mater. Bio.*, **2**, 121 (2008).
21. E. Sjöman, M. Mänttäri, M. Nyström, H. Koivikko and H. Heikkilä, *J. Membr. Sci.*, **310**, 268 (2008).
22. B. Qi, J. Luo, X. Chen, X. Hang and Y. Wan, *Bioresour. Technol.*, **102**, 7111 (2011).
23. F. Zhou, C. Wang and J. Wei, *Bioresour. Technol.*, **131**, 349 (2013).
24. F. Zhou, C. Wang and J. Wei, *J. Membr. Sci.*, **429**, 243 (2013).
25. M. Tanaka, M. Fukui and R. Matsuno, *Biotechnol. Bioeng.*, **32**, 897 (1988).
26. J. S. Knutsen and R. H. Davis, *Appl. Biochem. Biotechnol.*, **113-116**, 585 (2004).
27. J. Leberknight, B. Wielenga, A. Lee-Jewett and T. J. Menkhaus, *J. Membr. Sci.*, **366**, 405 (2011).
28. Bekaert Advanced Filtration SA, *Developing new media based on short metal fibres*, Retrieved from www.bekaert.com/baf (11/05/2014).
29. K. Matsumoto, S. Katsuyama and H. Ohya, *Ferment. Technol.*, **65**, 77 (1987).
30. G. Schulz and S. Ripperger, *J. Membr. Sci.*, **40**, 173 (1989).
31. P. C. Carman, *Trans. Inst. Chem. Eng.*, **50**, 150 (1937).